A New Global Ionospheric Model

K. W. Yip and O. H. von Roos
Tracking and Orbit Determination Section

A new global ionospheric model has been successfully implemented. The daytime portion of this model provides one-way ionospheric range corrections that compare favorably with those derived from the Mariner Venus/Mercury (MVM'73) S- and X-band dual frequency doppler data. For elevation angles, γ, higher than 30 deg and solar zenith angle, X, less than 80 deg, this model provides calibrations accurate to a few centimeters. The calibrations provided by the nighttime model are also very reasonable. These, however, will have to be compared with the S/X data from Viking '75 for final confirmation.

It is interesting to note that the daytime ionospheric calibrations derived from the current calibration scheme, DIEN/TIEN, are fairly close to those given by the new global model, especially in the temporal variations and thus the doppler effects. In the daytime and for $\gamma \gtrsim 30$ deg and $X < 80$ deg, the calibrations from the two models agree almost exactly. However, for situations when γ is below 30 deg and X is larger than 80 deg simultaneously, as much as 12% ($\sim$70 cm, typically) improvement of the new model over DIEN/TIEN results.

The comparison between the nighttime model and DIEN/TIEN has been based on the one-way ionospheric range corrections for three passes near the Mariner 9 encounter with Mars in 1971 tracked at Goldstone. It is found that they can differ by over 30% (typically 20 cm). As mentioned, the confirmation of these nighttime calibrations awaits the availability of the Viking S/X dual frequency doppler data.

Finally, the ionospheric calibration effects on orbit determination provided by DIEN/TIEN, the global model, and the S/X data will be intercompared during the Viking Mission.

I. Introduction

It has been shown (Ref. 1) that the Chapman ionospheric electron content distribution (Ref. 2), which the ionospheric calibration model DIEN/TIEN (Ref. 3) uses for deep space probe tracking, is an inadequate representation of Earth's ionosphere for low elevation angles and large solar zenith angles. Moreover, this electronic distribution, which is used in the daytime model, may not be a good description for the nighttime ionosphere. To improve the DSN spacecraft tracking capability, a global ionosphere model (Ref. 1) has been developed. This model consists of three distinct parts: the daytime model, the nighttime model, and the dawn model. Physically, the daytime model consists of the situation when electron production in the ionosphere due to solar ultraviolet predominates. This differs from the Chapman model in that the curvature of Earth has been taken into account, thus avoiding the singularity in the Chapman model when the solar zenith angle, X, is close to 90 deg. The nighttime model encompasses the situation when recombination and diffusion of the ionospheric electrons dominate. Finally, the dawn model considers the transition from the nighttime model to the daytime model. This article reports on the implementation and application of the daytime and nighttime ionospheric models. It has also been shown that the duration of dawn in the ionosphere is so short (~5 min) that the implementation of this part of the model is not necessary.

II. Mathematical Background of the Daytime Ionospheric Model

Several assumptions are involved in the development of the daytime model:

(1) N, the number density of the ionospheric neutral species obey an exponential law, i.e.,

$$N = N_0 \exp\left[-\left(\frac{r - R_e}{H}\right)\right]$$

where

N_0 = number density at Earth's surface

R_e = radius of Earth

H = scale height of neutral species

(2) Macroscopic charge neutrality, i.e., $N_i = N_e$ where the subscripts i and e represent ions and electrons, respectively.

(3) Stationary condition, i.e., $(d/dt)\, N_e = 0$

With these assumptions, the electronic distribution as a function of geocentric distance, r, is

$$N_e(r) = k_1 \exp\left\{\frac{1}{2}\left[-\frac{r - R_e}{H} + k_2 \int_\infty^r \exp\left(-\frac{x - R}{H}\right)\left(1 - \frac{y_0^2 + z_0^2}{x^2}\right)^{-1/2} dx\right]\right\} \tag{1}$$

where k_1 and k_2 are constants involving the ultraviolet absorption cross sections, recombination coefficients, and other physical parameters of the air molecules and solar radiation, and y_0 and z_0 are the Cartesian coordinates in a Sun-fixed coordinate system (Fig. 1).

The first principle quantities (k_1, k_2) in Eq. 1 are then linked to the Chapman parameters of a Chapman ionosphere, which is given by

$$\overset{\text{Chap}}{N_e}(Z) = N_{e_{max}} \exp\left\{\frac{1}{2}\left[1 - Z - \sec X \exp(-Z)\right]\right\} \tag{2}$$

where

$$Z = \frac{r - R_e - h_{max}}{H}$$

X = solar zenith angle, angle between the direction of the Sun's rays and the observer's zenith,

$N_{e_{max}}$ = maximum electron concentration at altitude $h = h_{max}$ and for $X = 0$

H = scale height of the ionosphere.

In other words, $X = 0$ in Eq. (2) corresponds to $y_0 = z_0 = 0$ in Eq. (1). Thus

$$N_e(\gamma) = N_{e_{max}} \exp\left\{\frac{1}{2}\left[1 - Z + \int_\infty^z \frac{\exp(-x)}{\left(1 - \frac{y_0^2 + z_0^2}{(Hx + R_e + h_{max})^2}\right)^{1/2}} dx\right]\right\} \tag{3}$$

where

$$y_0 = (HZ + R_e + h_{max}) \sin\theta_0 \sin\phi_0$$

$$z_0 = (HZ + R_e + h_{max}) \cos\theta_0$$

with ϕ_0 and θ_0 the longitude and colatitude in the Sun-fixed coordinate system (Fig. 1).

It has been shown (Ref. 4) that the range correction due to a tenuous plasma is given by

$$\Delta\rho = \frac{2\pi e^2}{m\omega^2}\int_{R_e} dr\left(1 - \frac{R_e^2\cos^2\gamma}{r^2}\right)^{-1/2} N_e(s(r)) \qquad (4)$$

The additional symbols in Eq. (4) are defined as: $s(r)$, the unperturbed (straight) ray path between the Earth-bound station and the distant spacecraft expressed as a function of r, which is the distance from the center of Earth; and γ, the elevation angle. In principle, therefore, Eq. (3) and Eq. (4) combined yield the ionospheric range change along any tracking station (location θ_0, ϕ_0)—spacecraft line of sight.

Now the Sun-fixed coordinates y_0, z_0 can be related to the Sun-fixed geographic locations θ_0, ϕ_0 and the elevation and azimuth angles γ and α. All these in turn can be transformed back into the usual Earth-fixed coordinate system. The details of this are outlined in Ref. 1 and are not repeated here. Only a summary of the relevant equations is displayed below:

$$S = -R_e \sin\gamma + \sqrt{r^2 - R_e^2 cos^2\gamma} \qquad (5)$$

$$y_0 = S(\sin\gamma \sin\theta_0 \sin\phi_0 - \cos\gamma \cos\alpha \cos\theta_0 \sin\phi_0 + \cos\gamma \sin\alpha \cos\phi_0) + R_e \sin\theta_0 \sin\phi_0 \qquad (6)$$

$$z_0 = S(\sin\gamma \cos\theta_0 + \cos\gamma \cos\alpha \sin\theta_0) + R\cos\theta_0 \qquad (7)$$

$$\cos\theta_G = \sin\delta_\odot \sin\theta_0 \cos\phi_0 + \cos\delta_\odot \cos\theta_0 \qquad (8)$$

$$\sin\theta_G \cos\phi_G = -\cos T \sin\delta_\odot \cos\theta_0 + \cos T \cos\delta_\odot \sin\theta_0 \cos\phi_0 - \sin T \sin\theta_0 \sin\phi_0 \qquad (9)$$

$$\sin\gamma \cos\theta_G + \cos\gamma \cos\alpha_G \sin\theta_G = \sin\delta(\sin\gamma \sin\theta_0 \cos\phi - \cos\gamma \cos\alpha \cos\theta_0 \cos\phi_0 - \cos\gamma \sin\alpha \sin\theta + \cos\delta(\sin\gamma \cos\theta_0 + \cos\gamma \cos\alpha \sin\theta_0) \qquad (10)$$

For these equations, the subscript 0 refers to quantities in the Sun-fixed coordinate system whereas the subscript G refers to quantities in the Earth-fixed coordinate system. γ, the elevation angle, is the same in both systems while the azimuth is transformed from α to α_G. $\delta_\odot$ is the declination of the Sun and $T \equiv 12^h - UT$ is the time coordinate.

III. Implementation of the Daytime Ionospheric Model

The daytime ionospheric model has been used to map the ionospheric total electron contents from a station-geostationary satellite ray path to the station-spacecraft ray path. As is the case with the old ionospheric model DIEN/TIEN, the input Faraday rotation data are space-time translated and then mapped to the desired elevation angle, γ. This elevation angle mapping is accomplished by the multiplication of the ratio of the range change at γ to that at $\gamma = 90$ deg. However, the elevation angle mapping of the new model does not involve the ray-trace solutions through a Chapman ionosphere. This avoids the inadequacies of the Chapman ionospheric representation at large solar zenith angles and low elevation angles of the old model. The magnetic latitude adjustments are again applied in a similar manner.

A computer program has been coded for the implementation of the daytime ionospheric model. The boundary of the "daytime" ionosphere is defined conservatively. Figure 2 shows a schematic Earth in the Sun-fixed coordinate system. A tracking station S is considered to be tracking in the daytime only if $|\phi_0| \leq 90$ deg. This is conservative since for the situation illustrated in the figure, no calibration will be provided even though the tracking is still done in the daytime ionosphere. This conservative "cut-off" does not affect the following comparisons.

IV. Validity of the Daytime Ionospheric Model

During the MVM'73 mission, both S- and X-band doppler data were available. Thus the station-spacecraft line-of- sight charged particle contents (i.e., both of ionospheric and space plasma origin) were readily deduced (Ref. 5). The three earliest S/X dual-frequency passes in the mission have been chosen in the comparison with the calibrations provided by the daytime ionospheric model.

Due to the proximity of the spacecraft to Earth for these three passes, the significance of solar plasma contribution to the line-of-sight charged particle content is probably minimal. Moreover, the calibrations provided by these three passes have been compared in detail with those

provided by the old ionospheric calibration program DIEN/TIEN (Ref. 6). Thus, the improvement, if any, of the new daytime model over the old one can be deduced as well.

Figures 3, 4, and 5 show the comparisons of the charged particle calibrations provided by the S/X dual-frequency doppler data and the new daytime ionospheric model. The calibrations given for DIEN/TIEN are also plotted on the same figures for comparison. Except for the beginning and end portions of the second pass (Dec. 30, 1973), the old and new models yield almost identical one-way ionospheric range changes.

1. Pass 1: December 15, 1973. The first S/X data of suitable quality were obtained at DSS 14 on December 15, 1973 (Fig. 3). The data spans ~6 h. They reveal a long term decrease in the line-of-sight electron content: a 1-m decrease over the 6-h interval. In addition to the long-term signature, there is also a repetitive short-term structure (~40 min from one local maximum to the next). These short-term structures have been found to be correlated with the roll limit cycle of the spacecraft by B. W. Dysart and W. L. Martin. Modification of the experimental dual frequency receivers at the Mars Station, Goldstone, corrected this problem. Subsequent S/X data passes do not show this repetitive structure.

Table 1 shows the prevalent elevation angle, γ, and solar zenith angle, X, for the beginning and end portions of the three passes. It can be seen that for this first pass, when the elevation angle is fairly low ($\lesssim 30$ deg), the solar zenith angle is not excessively high ($\lesssim 60$ deg). Thus reasonable ionospheric modeling should result (Ref. 1) and, as expected, the agreement between the S/X and the new ionospheric calibrations is good to ~10 cm throughout the entire pass.

Table 2 shows the values of the Chapman parameters on this day obtained by means of ionosonde data from Point Arguello, California, and White Sands, New Mexico. Figure 6 displays the variations of the ionospheric reference points (Ref. 3) between the station-spacecraft ray path on this day and the two ionosonde data sources. Since rather significant uncertainties could be involved in ionosonde measurements (Ref. 7), constant values of 250 km and 39 km have been used, respectively, for the Chapman parameters h_{max} and H in the computation of one-way range effects from the daytime model on this day (Eq. 3 and 4). Moreover, these numbers are approximate averages of those observed at the two ionosonde sites.

The mapped Faraday rotation data assess only the total electron content of the ionosphere along the station-spacecraft line of sight, while the S/X dual doppler data assess the variation of the electron content of the ionosphere and the space plasma collectively. Since the S/X and Faraday data yield electron contents that do not drift relative to each other by more than 0.2 m, the plasma must not exceed this level during the 6-h period of this pass.

Since the Faraday data have to be mapped over a distance of more than 1500 km (~13 deg in angular separation at the ionospheric reference points) in the beginning of the pass, and more than 350 km (~3 deg in angular separation) at the end of the pass, the fine structure variations along the station-spacecraft ray paths are not expected to be accounted for by the "mapped" Faraday data. As seen in Fig. 3, the short-term variations of the Faraday and S/X data do not correlate, and the maximum difference is < 0.2 m.

2. Pass 2: December 30, 1973. Again, the relevant elevation and solar zenith angles for this pass are shown in Table 1. Towards the end of the pass, low elevation angles ($\lesssim 30$ deg) are accompanied by large solar zenith angles ($\gtrsim 90$ deg). As expected, the new and old ionospheric models diverge the most ($\lesssim 10$ cm) towards the end of the pass, with the new model in better agreement with the S/X data. Since the old model is based on a Chapman ionospheric profile, which is known to be inadequate for $X \gtrsim 85$ deg (Ref. 2), the disagreement between the old model and the S/X data is not too surprising. The new model, however, should be valid for the entire daytime ionosphere. Thus, it is likely that the S/X data are detecting space plasma variations as well as those of the ionosphere. Figure 4 reveals that the S/X electron content is higher than the Faraday electron content in the beginning of the pass while the reverse is true for the end of the pass. Recalling that the S/X data measure only the time rate of change of the line-of-sight electron content, while the Faraday data measures the absolute line of sight total electron content, the disagreement can be explained by having a plasma cloud entering the station-spacecraft ray path in the beginning of the pass and leaving it towards the end.[1] Since the motion of the cloud relative to Earth is not known, the size of the cloud cannot be ascertained. The existence of a plasma

[1]This explanation is plausible because the Earth-spacecraft distance has been 15×10^6 km on this day. Typical plasma cloud dimensions are of the order of 10^6 km. Therefore, a plasma cloud may well have entered the ray path without engulfing Earth and affecting the ionosphere.

cloud drifting across the station-spacecraft ray path however, can explain the disagreements between the Faraday and S/X calibrations observed during this pass.

It should be noted that constant values of 250 km and 39 km have been adopted again for the parameters h_{max} and H (Table 3). Attempts made to account for the disagreements between the Faraday and S/X data by varying these parameter values have not succeeded. It has been found that the sensitivity of the one-way range change on the parameter H is very small. Moreover, an increase of h_{max} from 250 km to 350 km decreases the range change at UT $\simeq 24^h70$ ($\gamma \cong 36$ deg) by only $\lesssim 1\%$, for example. Thus, uncertainties in the parameter values cannot cause the discrepancies. The existence of space plasma seems to be a very plausible explanation.

3. Pass 3: January 3, 1974. Table 1 shows the relevant angular information for this pass and Fig. 5 displays the three calibrations. The agreements between these calibrations are excellent. This stems from two developments: DSS 14 S/X hardware had been modified and the data were taken at a more favorable geometry, i.e., elevation angles were higher ($\gtrsim 40$ deg) and the Faraday data had to be mapped over a shorter distance ($\lesssim 6$ deg in angular separation of the ray paths). The maximum difference between the mapped Faraday and the S/X measurements is < 0.05 m.

V. Mathematical Background of the Nighttime Ionospheric Model

In Ref. 1, the electron density approximately applicable at high altitudes ($\gtrsim 300$ km) as a function of time and height is given by

$$\frac{\partial N}{\partial t} = \alpha \exp(z)\left(\frac{\partial^2 N}{dz^2} + \frac{3}{2}\frac{\partial N}{\partial z} + \frac{1}{2}N\right) - \beta \exp(-z)\, N \tag{11}$$

where the first term on the right-hand side of the equation is responsible for the diffusion and the second term for attachment (α and β are the diffusion and recombination coefficients respectively). These are the only processes assumed to be occurring in the ionosphere at nighttime. Solving this linear differential equation, the solution is found to be the summation of a series of Laguerre polynomials, with the constants determined by matching the boundary conditions with the daytime ionospheric electron distribution at dusk. It has been found, however, that for most cases, this sum converges slowly. It is therefore not suitable for analytic applications. However, this series can be summed in closed form. Thus, the nighttime ionospheric electron profile is then given by:

$$\begin{aligned} N(z,t) = {} & \left(\frac{\beta}{\alpha}\right)^{1/4} N_{\max} \exp\frac{1}{2}\left\{\left(1 + \frac{h_{max}}{H}\right)\right\} (1-X)^{-1/2} \\ & \times \left(A + \frac{X}{1-X}\right)^{-1/2} \exp\left\{-z - \frac{1}{2}Y\right\} (XY)^{-1/2} \\ & \times \exp\left\{-\frac{3}{2}\sqrt{\alpha\beta}\, t + Z - XY/(1-X)\right\} \\ & \times \{2\,\mathrm{erf}(\sqrt{Z})\} \end{aligned} \tag{12}$$

where

$$z = \frac{r-R}{H}$$

$$Z = XY/\{(1-X)^2 A + X(1-X)\}$$

$$X = \exp\{-2\sqrt{\alpha\beta}\, t\}$$

$$Y = 2\sqrt{\beta/\alpha}\exp(-z)$$

$$A = \frac{1}{2}\left(1 + \sqrt{\frac{\pi R\alpha}{2H\beta}}\exp\left(\frac{h_{max}}{H}\right)\right)$$

and

R = radius of Earth

H = ionospheric scale height

α = diffusion coefficient of electrons in s^{-1} (see Ref. 1)

β = attachment coefficient of electrons in s^{-1} (see Ref. 1)

t = time in seconds from dusk

h_{max} = height above ground where electron density distribution is maximum

N_{max} = maximum electron concentration at altitude $h = h_{max}$ and for solar zenith angle, X, = 0.

Note that the parameters H, h_{max}, N_{max} appear due to the matching of boundary conditions between the daytime and nighttime ionospheres at dusk. In terms of the geocentric distance, r, this electronic distribution can be written as

$$\begin{aligned} N(r,t) = {} & N_{max} \exp\left[\frac{1}{2}\left(1 + \frac{h_{max}}{H}\right)\right][AX(1-X) + X^2]^{-1/2} \\ & \times \exp\left[-\frac{3}{2}\sqrt{\alpha\beta}\, t\right]\exp\left\{-\frac{1}{2}\left(\frac{r-R}{H}\right)\right. \\ & \left. + \sqrt{\frac{\beta}{\alpha}}\left[\frac{X - A(1+X)}{X + A(1-X)}\right]\exp\left(\frac{r-R}{H}\right)\right\}\mathrm{erf}(\sqrt{Z}) \end{aligned} \tag{13}$$

Thus, the range change, $\Delta\rho$, due to this nighttime ionospheric electron distribution is

$$\Delta\rho(t) = \frac{2\pi e^2}{m\omega^2} N_{max} \exp\left[\frac{1}{2}\left(1+\frac{h_{max}}{H}\right)\right]\{AX(1-X)+X^2\}^{-1/2} \times \exp\left[-\frac{3}{2}\sqrt{\alpha\beta}(UT - T_{90})\right] \times \int_R^\infty dr\left(1-\frac{R^2\cos^2\gamma}{r^2}\right)^{-1/2} \exp\left\{-\frac{1}{2}\left(\frac{r-R}{H}\right) + \frac{\beta}{\alpha}\left[\frac{X-A(1+X)}{X+A(1-X)}\right]\exp\left(-\frac{r-R}{H}\right)\right\} \operatorname{erf}(\sqrt{Z}) \quad (14)$$

where $T_{90} = \cos^{-1}(\tan\delta_\odot \cot\theta_G) - \phi_G + \pi$ is the universal time when the tracking station in question has a "Sun-fixed" station longitude equal to $\pi/2$ (see Section III). In other words, nighttime ionospheric condition prevails from this time on.

Furthermore,

$\delta_\odot$ = declination of the Sun.

θ_G = geographic tracking station co-latitude

ϕ_G = geographic tracking station longitude

Incidentally, Eq. (14) is, in appearance at least, very much different from the range change given by a Chapman-like electronic distribution. Thus, the ionospheric range changes resulting from the new nighttime model may be quite different from those given by DIEN/TIEN.

VI. The Diffusion and Recombination Coefficients

The implementation of the nighttime ionospheric model depends on obtaining reasonable values for the diffusion and recombination coefficients α and β. Unfortunately, as mentioned in Ref. 8, these values are quite uncertain. They not only depend on the exact knowledge of the composition in the upper ionosphere, but also on the knowledge of the exact diffusion and recombination rates. At a 300-km altitude they are given as $1.95 \times 10^{-4}s^{-1}$, $2.6 \times 10^9 cm^2/s$, and $4 \times 10^{-4}s^{-1}$, $2 \times 10^{10}cm^2/s$ respectively for moderate levels of solar activity. Although attempts (Ref. 11) to explain the order of magnitude difference between the experimental value of α by Quinn, et al. (Ref. 9), and the theoretical value by Risbeth, et al. (Ref. 10), have been made, the situation is still very uncertain due to the lack of the exact knowledges mentioned above. Moreover, since these conditions are quite variable from region to region, it would only seem reasonable to use the α and β values that are determined locally. As a matter of fact, as will be shown below, the evaluation of the ionospheric one-way range changes using the "best" values of α and β from Quinn, et al., yields unacceptable results.

The following procedure illustrates how the values of α and β can be determined for Goldstone using the zenith total electron content (TEC) data measured at Goldstone, and Eq. (13).

The time dependence of the zenith TEC as given by Eq. (13) is fairly complex. Note that the time dependence is contained in the parameters X and Z and thus in the terms $\{AX(1-X)+X^2\}^{-1/2}$ erf $(\sqrt{Z})$, exp $-(3\sqrt{\alpha\beta}\,t)/2$ and exp $\sqrt{\beta/\alpha}\,[X - A(1+X)]/[X + A(1-X)]$. Fortunately, it can be shown that for the nighttime ionosphere, i.e., $0 \leq t \lesssim 12$ h, the first and third terms vary fairly slowly in comparison to the second one, exp $-(3\sqrt{\alpha\beta}\,t)/2$. This is confirmed by the actual zenith TEC measurements. Figures 7 and 8 show four days (November 11, 12, 13, and 14, 1971) of zenith TEC observed in Goldstone. These TECs are plotted on semi-log scales. Except for November 12 (more discussion on this day later), an exponential decay in the zenith TEC is clearly indicated after T_{90} (footnote 2), confirming that exp $-(3\sqrt{\alpha\beta}\,t)/2$ is the dominating factor. Moreover, it can also be shown that while the first and third terms vary by factors of two or three over the whole night, the exponential decaying factor varies by two to three orders of magnitude. Thus it can be concluded that the decay has the slope roughly equal to $1.5\sqrt{\alpha\beta}$.

It is obvious that a constant set of α and β cannot be used for the entire night. If this were the case, changes in range of two to three orders of magnitude would be expected, and this would not agree with the observations. As can be deduced from Figs. 7 and 8, the first set is applicable only for a few hours after dusk. A second (or maybe even third set) will have to be applied later during the night.

Before discussing the second and/or third set of values for α and β, investigation will now be made on the values for the first set, i.e., the set applicable from around dusk on. Since only the product $\alpha\beta$ (Table 4) can be determined from the measured zenith TEC data, another independent determination has to be available. The clue

[2]The beginning of night.

to this determination comes from the observation that the value of β seems to be more consistent from different sources (e.g., Refs. 9 and 10). Thus, the approach here is to adopt a published value for β and then determine the value of α from the derived product of α and β. Moreover, to justify the validity of the above approach and to obtain an idea for the uncertainty of the resultant range change, computations for other values of β (variations over a decade, 0.5 s^{-1} to 5 s^{-1}) and their corresponding values of α have been used in the determination of $\Delta\rho$. Table 5 shows the range corrections for the different α and β values for the three nights under investigation. The daytime range changes have also been computed (Section III) for comparison. It is seen that the variation in $\Delta\rho$ due to the different α and β values is reasonably small ($\lesssim$15%, $\sim$12 cm). Besides, the variation in β is usually much less than an order of magnitude anyway.

β and α in Eq. (13) can also be obtained from published values by the multiplication of the factor exp $\pm(300/H)$ (footnote 3). Note that different signs apply to α and β since recombination decreases with increases of altitude (from $\sim$300 km upward) while the reverse is true for diffusion. It should also be noted that, following Quinn, et al. (Ref. 9), the scale height H is taken to be 33 km for the recombination process and 66 km for the diffusion process.[4] Table 6 shows the α and β values thus derived. As mentioned, the corresponding range corrections are unacceptably large.

Table 4 also shows decaying exponents for other parts of the night for November 11, 13, and 14. Note that within the framework of the present nighttime model, an increase in zenith TEC cannot be accounted for. This is the reason why the evaluation for the nighttime ionospheric range change for November 12 has been omitted.[5]

Now, the knowledge of the values for α and β during the so-called 'night-stationary' conditions (Ref. 10) are even less understood. However, as will be shown later, when the product of α and β takes on such small values, it does not matter much what the exact values of α and β are. Table 7 shows the range changes for the other parts of the nights with α and β taking on arbitrary values but keeping their products fixed. For the November 14 pass, the second slope is so close to zero that the product α and β is several orders of magnitude smaller than the values obtained for the other two nights. Incidentally, it is interesting to note that when the values of α and β are small enough, as in the case of November 14, further decrease in their product values causes no variation in the one-way range changes. It should be noted, however, that although no major variations have been obtained using these arbitrary values of α and β, this lack of an exact knowledge and the resulting differences in $\Delta\rho$ ($\gtrsim$0.1 m) set a limit to the accuracy of range change evaluation for the second and subsequent portions of the nighttime ionosphere.

VII. Nighttime Ionospheric One-Way Range Changes

Figures 9, 10, and 11 show the one-way range changes due to the nighttime ionosphere on November 11, 13, and 14 in 1971 for the spacecraft Mariner 9 tracked by DSS 14 at Goldstone. The daytime portion of the ionospheric range changes have been computed using the new daytime model (Section III). Note that due to the unfavorable elevation angle ($\lesssim$35 deg) and solar zenith angle ($\gtrsim$90 deg) geometry, the improvement of the daytime model over DIEN/TIEN ($\lesssim$70 cm) is more apparent. Different values of α and β are also indicated. It is seen that the values of α and β can vary by factors of two and still yield reasonable one-way range changes. It seems that this uncertainty can be resolved only when S/X dual-frequency doppler data from the spacecraft become available in the nighttime. The gap between the day and night range changes is due to the loss of precision of the computer when the integration of the daytime model gets to be too close to dusk. Attempts will be made to improve on this. Incidentally, when this gap gets to be sufficiently small, it may be possible to select out the nighttime curve for the proper values of α and β. Note also that one-way range points from the current ionospheric calibration technique DIEN/TIEN have also been plotted. Although magnitude-wise, the difference between the new nighttime model curve and the DIEN/TIEN curve may be fairly small ($\sim$22 cm), the fractional difference is quite large ($\gtrsim$30%) due to the smaller range changes in the nighttime ionosphere.

It should be pointed out that a preliminary study in the improvement of the tracking doppler residuals by

[3]The reason for the factor exp $\pm(300/H)$ is the fact that both α and β have been given for h = 300 km and have to be scaled accordingly for any other altitude.

[4]Diffusion scale height for electrons = two times scale height for neutrals (Ref. 12).

[5]The reason for the increase in TEC later during the night on November 12 can be explained only by lateral motion of the upper atmospheric gas masses or cosmic ray bursts. Such effects have not been incorporated into the present model.

means of the ionospheric calibrations from these three passes are rather inconclusive. More passes of calibration with the new global ionospheric model will be evaluated and the results will be published in a future article.

VIII. Ionospheric Model at Dawn

As was pointed out earlier, the duration of twilight (Fig. 12) in the upper ionosphere at midlatitudes either north or south from the equator is rather short. This means that the transition from complete darkness to complete daylight in the F layer of the ionosphere may be neglected as far as range correction computations are concerned, thus saving considerable time and effort.

It has been shown (Ref. 1) that the duration of twilight is given by the expression:

$$\tau_t = \dot{\theta}^{-1} \sin^{-1} \left\{ \frac{\cos \delta_\odot}{\sin \theta_G} \left[\left(2 \frac{h_{max} + H}{R} \right)^{1/2} - \left(2 \frac{h_{max}}{R} \right)^{1/2} \right] \right\} \tag{15}$$

Here τ_t is the duration of twilight. $\delta_\odot$ is the declination of the sun, θ_G the geographical colatitude, h_{max} the altitude of maximum electron density, H the scale height of the F layer, R is the radius of Earth, and $\dot{\theta} = 7.3 \times 10^{-5}$ rad/s, Earth's spin rate. Taking nominal values for h_{max}, H, and R (i.e., $H = 39$ km, $h_{max} = 250$ km, $R = 6370$ km) we find:

$$\tau_t = 1.4 \times 10^4 \sin^{-1} \left\{ 0.021 \frac{\cos \delta_\odot}{\sin \theta_G} \right\} \text{[s]}) \tag{16}$$

Table 8 shows a list of the twilight durations τ_t for $\theta_G = 60$ deg, the approximate colatitude of the DSN stations as a function of $\delta_\odot$.

We therefore see that the transition time between night and day is rather short. The reason for this is the fact that only geometrical factors enter the derivation of Eq. (15), since light scattering is negligible because of the low density of matter ($\ll 10^{14}$ atoms/cm^3). In other words, shadows are sharp.

IX. Conclusion

On the basis of the comparisons with the S/X dual-frequency doppler data from MVM'73, it can be concluded that as the old model DIEN/TIEN, the new daytime ionospheric model is capable of calibrating the station-spacecraft ray-path ionospheric total electron content to a few centimeters for elevation angles $\gtrsim 30$ deg and solar zenith angles $\lesssim 80$ deg. However, for elevation angles below 30 deg and solar zenith angles larger than 80 deg simultaneously, the new model can improve the ionospheric calibration by as much as 12% over the old model. Nevertheless, the doppler calibrations provided by both models are quite similar. As mentioned, both models usually cannot account for fine structure variations along the tracking station-spacecraft ray path.

As for the nighttime ionospheric model, although there are slight uncertainties in the exact values for the diffusion and recombination constants α and β, the nighttime range changes join smoothly to the range changes generated from the new daytime ionospheric model. Moreover, the range corrections computed by the new nighttime model may differ by over 30% (~20 cm) from the currently used calibration technique DIEN/TIEN.

The one-way range changes from the nighttime model will be compared with those deduced from the Viking S/X dual-frequency doppler data when the latter become available. Also, the effects of the entire new global ionospheric model on the doppler tracking data and orbit determination will be checked out and published in a future article.

References

1. von Roos, O. H., Yip, K. W., Escobal, P. R., "A Global Model of the Earth's Ionosphere for Use in Space Applications," *Astronautica Acta*, Vol. 18 (Supp.), p. 215, 1974.

2. Chapman, S., "The Absorption and Dissociative or Ionizing Effect of Monochromatic Radiation in an Atmosphere on a Rotating Earth," *Proc. Phys. Soc.* (London), Vol. 43, p. 25, 1931.

3. Yip, K. W., Winn, F. B., Reid, M. S., Stelzried, C. T., "Decimeter Modeling of Ionospheric Columnar Electron Content at S-Band Frequencies," paper presented at the Ionospheric Effects Symposium, Jan. 20-22, 1975, sponsored by the Naval Research Laboratory, Washington, D. C.

4. von Roos, O. H., "Tropospheric and Ionospheric Range Corrections for an Arbitrary Inhomogeneous Atmosphere (First Order Theory)," *The Deep Space Network Progress Report*, Technical Report 32-1526, Vol. VI, p. 99. Jet Propulsion Laboratory, Pasadena, Calif., Dec. 1971.

5. Madrid, G. A., "The Measurement of Dispersive Effects Using the Mariner 10 S- and X-Band Spacecraft to Station Link," *The Deep Space Network Progress Report 42-22*, p. 22. Jet Propulsion Laboratory, Pasadena, Calif., May 1974.

6. Winn, F. B., Yip, K. W., Reinbold, S. J., "DSN-MVM'73 S/X Dual Frequency Doppler Demonstration," *The Deep Space Network Progress Report 42-22*, p. 28. Jet Propulsion Laboratory, Pasadena, Calif., May 1974.

7. Wright, J. W., Smith, G. H., "Review of Current Methods for Obtaining Electron-Density Profiles from Ionograms," *Radio Science*, Vol. 2, p. 1119, Oct. 1967.

8. Rishbeth, H., "A Review of Ionospheric F Region Theory," *Proc. of IEEE*, Vol. 55, p. 16, January 1967.

9. Quinn, T. P., Nisbet, J. S., "Recombination and Transport in the Nighttime F Layer of the Ionosphere," *J. Geophys. Res.*, Vol. 70, p. 113,, Jan. 1965.

10. Rishbeth, H., Garriott, O. K., *Introduction to Ionospheric Physics*, Academic Press, New York and London, 1969.

11. Shimazaki, T., "Nighttime Variations of F-Region Electron Density Profiles at Puerto Rico, 2. An Attempt to Separate the Effects of Temperature Variation and Drift Velocity," *J. Geophys. Res.*, Vol. 71, p. 3177, July 1966.

12. Ferraro, V. C. A., "Diffusion of Ions in the Ionosphere," *Terr. Magn. Atmos. Elect.*, Vol. 50, p. 215, 1945.

Table 1. Elevation and solar zenith angles for the first three S/X passes

Date	Time (UT), h	Elevation angle γ, deg	Solar zenith angle X, deg
12/15/73	18.30	16.79	58.55
	18.78	22.62	58.65
	19.21	27.63	58.90
	⋮	⋮	⋮
	23.30	57.70	78.85
	23.47	57.39	80.20
	23.65	56.86	81.65
12/30/73	19.13	39.21	58.3
	19.50	42.81	58.5
	⋮	⋮	⋮
	24.70	35.96	87.65
	25.08	31.79	90.50
	25.48	27.31	93.35
	25.92	22.24	96.15
1/3/74	19.36	43.80	58.05
	19.54	45.38	58.15
	⋮	⋮	⋮
	22.08	52.44	67.45
	23.82	40.27	79.70

Table 2. Chapman parameters h_{max} and H for Dec. 15, 1973

Ionosonde site	Time (UT), h	H_{max}, km	H, km
Point Arguello, Calif.	17:00	231	34
	17:30	218	39
	18:00	229	31
	18:30	239	46
	19:00	241	43
	19:30	255	36
	20:00	241	50
	20:30	238	34
	21:00	228	42
	21:30	239	53
	22:00	245	40
	22:30	251	57
	23:00	219	23
	23:30	233	40
	24:00	272	52
	0:30	256	52
	1:00	247	31
White Sands, New Mexico	17:00	219	43
	17:30	259	45
	18:00	230	32
	18:30	219	37
	19:00	254	43
	19:30	221	20
	20:00	226	43
	20:30	231	
	21:00	221	27
	21:30	233	30
	22:00	234	33
	22:30	227	36
	23:00	235	33
	23:30	238	40
	24:00	250	35
	0:30	245	38
	1:00	241	36

Table 3. Chapman parameters h_{max} and H for Dec. 30, 1973

Ionosonde site	Time (UT), h	h_{max}, km	H, km
Point Arguello, Calif.	18:00	252	39
	18:30	267	47
	19:00	253	39
	19:30	251	38
	20:00	266	49
	20:30	248	46
	21:00	262	59
	21:30	232	28
	22:00	228	34
	22:30	227	30
	23:00	221	35
	23:30	224	45
	24:00	243	43
	0:30	230	35
	0:45	226	39
	2:00	274	45
White Sands. New Mexico	18:00	250	41
	18:30	249	39
	19:00	274	46
	19:30	250	31
	20:00	232	33
	20:30	244	42
	21:00	245	33
	21:30	231	30
	22:00	220	41
	22:30	223	28
	23:00	226	33
	23:30	237	46
	24:00	264	54
	0:30	244	36
	1:00	264	41
	1:30	295	43
	2:30	303	34

Table 4. Summary of $\alpha\beta$ values

Date	Time span, h	$\alpha\beta$, s^{-2}
11/11/71	26.70–28.3	$\sim 1.18 \times 10^{-8}$
	28.3 –29.35	$\sim 2.02 \times 10^{-10}$
	29.35 on	undefined
11/13/71	26.71–29.4	$\sim 1.97 \times 10^{-9}$
	29.4 on	$\sim 2.70 \times 10^{-12}$
11/14/71	26.71–29.0	$\sim 4.92 \times 10^{-10}$
	29.0 –31.0	~ 0

Table 5. Ionospheric one-way range changes

Date	UT	Elevation, deg	Δρ, m: New daytime model	Δρ, m: Nighttime model				Δρ, m: DIEN/TIEN
11/11/71	21.99	7.06	5.23					4.63
	22.87	16.86	3.61					3.21
	23.53	23.72	2.66					2.99
	24.14	29.41	1.99					1.64
	24.72	34.15	1.50					1.14
	25.28	37.96	1.11					0.73
	⋮			$\beta = 0.5$, $\alpha = 2.36 \times 10^{-8}$	$\beta = 1$, $\alpha = 1.18 \times 10^{-8}$	$\beta = 2$, $\alpha = 5.91 \times 10^{-9}$	$\beta = 5$, $\alpha = 2.36 \times 10^{-9}$	⋮
	26.93	42.68		0.66	0.65	0.66	0.72	0.44
	27.48	41.77		0.60	0.60	0.61	0.63	0.44
	28.03	39.64		0.59	0.59	0.59	0.60	0.46
	28.58	36.41		0.59[a]	0.59[a]	0.59[a]	0.59[a]	0.53
	29.15	32.19		0.60[a]	0.59[a]	0.59[a]	0.59[a]	0.49
	29.74	27.04		0.61[a]	0.60[a]	0.60[a]	0.59[a]	0.60
	30.36	20.90		0.62[a]	0.61[a]	0.60[a]	0.59[a]	0.71
	31.08	13.20		0.60[a]	0.59[a]	0.57[a]	0.56[a]	0.88
11/13/71	22.10	9.30	4.86					4.40
	22.90	18.24	3.44					3.09
	23.55	24.92	2.56					2.23
	24.15	30.47	1.93					1.60
	24.73	35.11	1.45					1.12
	25.29	38.80	1.07					0.71
	⋮			$\beta = 0.5$, $\alpha = 3.95 \times 10^{-9}$	$\beta = 1$, $\alpha = 1.97 \times 10^{-9}$	$\beta = 2$, $\alpha = 9.86 \times 10^{-10}$	$\beta = 5$, $\alpha = 3.95 \times 10^{-10}$	⋮
	26.93	43.06		0.52	0.53	0.55	0.63	0.44
	27.48	41.97		0.50	0.51	0.52	0.55	0.44
	28.03	39.67		0.51	0.51	0.52	0.53	0.46
	28.59	36.28		0.52	0.52	0.53	0.53	0.49
	29.16	31.91		0.55	0.55	0.55	0.55	0.54
	29.75	26.62		0.59[a]	0.59[a]	0.58[a]	0.58[a]	0.61
	30.38	20.31		0.65[a]	0.64[a]	0.63[a]	0.62[a]	0.72
	31.12	12.32		0.72[a]	0.70[a]	0.68[a]	0.66[a]	0.90
11/14/71	21.48	2.72	5.88					5.19
	22.56	15.02	3.93					3.59
	23.25	22.38	2.90					2.57
	23.87	28.36	2.18					1.87
	24.45	33.41	1.65					1.33
	25.01	37.52	1.24					0.90
	⋮			$\beta = 0.5$, $\alpha = 9.83 \times 10^{-10}$	$\beta = 1$, $\alpha = 4.92 \times 10^{-10}$	$\beta = 2$, $\alpha = 2.46 \times 10^{-10}$	$\beta = 5$, $\alpha = 9.83 \times 10^{-11}$	⋮
	26.94	43.24		0.48	0.49	0.52	0.60	0.43
	27.49	42.06		0.47	0.48	0.50	0.53	0.44
	28.04	39.68		0.48	0.49	0.50	0.51	0.46
	28.60	36.20		0.50	0.51	0.51	0.52	0.49
	29.16	31.76		0.54[a]	0.54[a]	0.54[a]	0.54[a]	0.54
	29.76	26.41		0.59[a]	0.58[a]	0.64[a]	0.58[a]	0.61
	30.39	20.01		0.66[a]	0.65[a]	0.64[a]	0.63[a]	0.72
	31.14	11.85		0.76[a]	0.74[a]	0.72[a]	0.70[a]	0.91

[a]Second (or third) set of α and β values should have been used.

Table 6. Values of α and β from Refs. 7 and 8

Source	α (s^{-1})	β (s^{-1})	Comment
Quinn, et al. (Ref. 10)	2.53×10^{-6}	1.73	Summer, moderate solar activity
Quinn, et al. (Ref. 10)	2.53×10^{-6}	0.80	Winter, moderate solar activity
Rishbeth, et al. (Ref. 11)	1.37×10^{-4}	0.05	Sunspot minimum
	1.95×10^{-5}	3.55	Sunspot maximum

Table 7. Ionospheric one-way range changes

Date	UT, h	Elevation, deg	$\Delta\rho$, m		DIEN/TIEN
			$\beta = 1$, $\alpha = 2.02 \times 10^{-10}$	$\beta = 10^{-4}$, $\alpha = 2.02 \times 10^{-6}$	
11/11/71	28.58	36.41	0.50	0.61	0.49
	29.15	32.19	0.53	0.61	0.53
	29.74	27.04	0.58[a]	0.64[a]	0.60
	30.36	20.90	0.65[a]	0.70[a]	0.71
	31.08	13.20	0.74[a]	0.80[a]	0.88
			$\beta = 1$, $\alpha = 2.7 \times 10^{-12}$	$\beta = 10^{-6}$, $\alpha = 2.7 \times 10^{-6}$	
11/13/71	29.75	26.62	0.58	0.64	0.61
	30.38	20.31	0.65	0.70	0.72
	31.12	12.32	0.76	0.81	0.90
			$\beta = 5$, $\alpha = 9.83 \times 10^{-15,17}$	$\beta = 8.2 \times 10^{-7,9}$, $\alpha = 6 \times 10^{-8}$	
11/14/71	29.16	31.76	0.53	0.56	0.54
	29.76	26.41	0.57	0.61	0.61
	30.39	20.01	0.63	0.71	0.72
	31.14	11.85	0.72	0.86	0.91

[a]Positive slope indicated in Fig. 1.

Table 8. Duration of twilight for DSS located at $|30$ deg$|$ latitude

τ_t [min]	δ_θ, deg
5.7	0
5.6	10
5.3	20

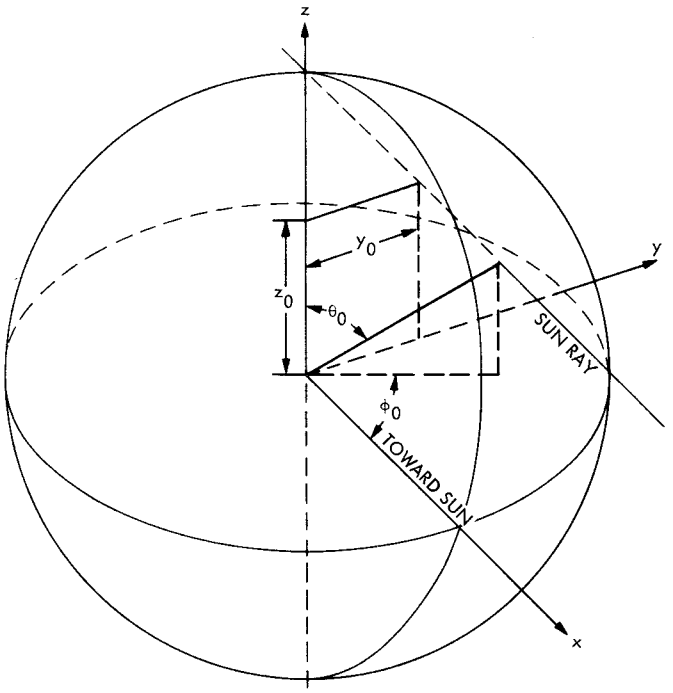

Fig. 1. Geometry of the system

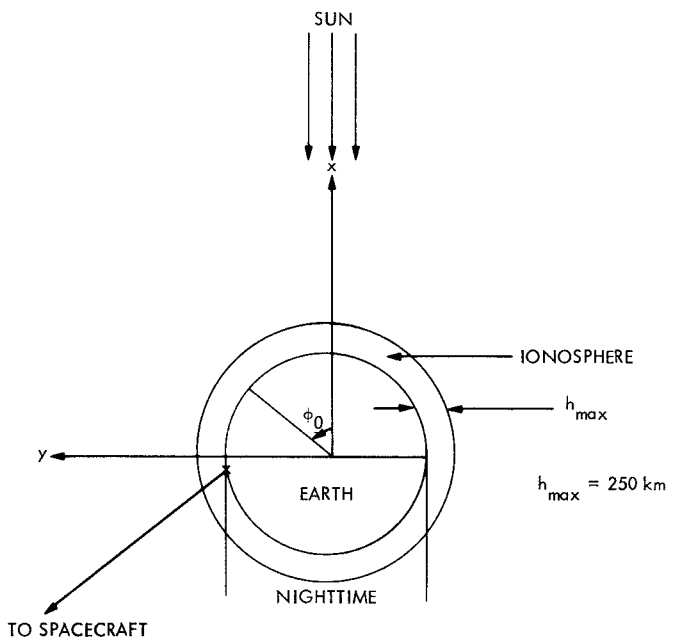

Fig. 2. Schematic of daytime and nighttime ionosphere

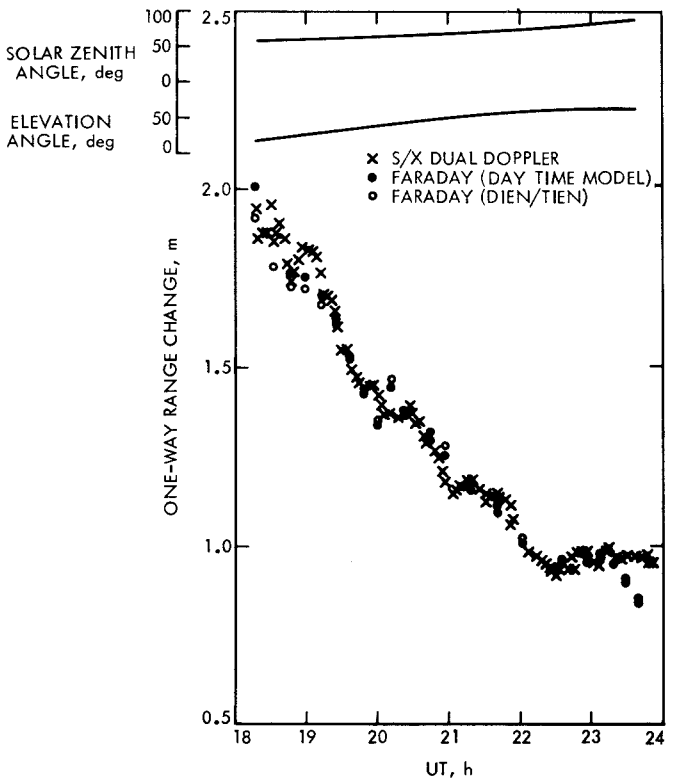

Fig. 3. Comparison of daytime ionospheric one-way range changes on Dec. 15, 1973

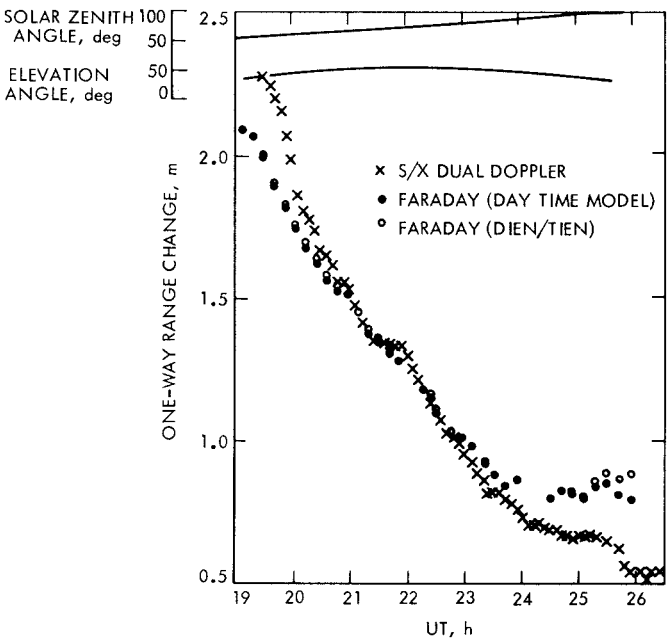

Fig. 4. Comparison of daytime ionospheric one-way range changes on Dec. 30, 1973

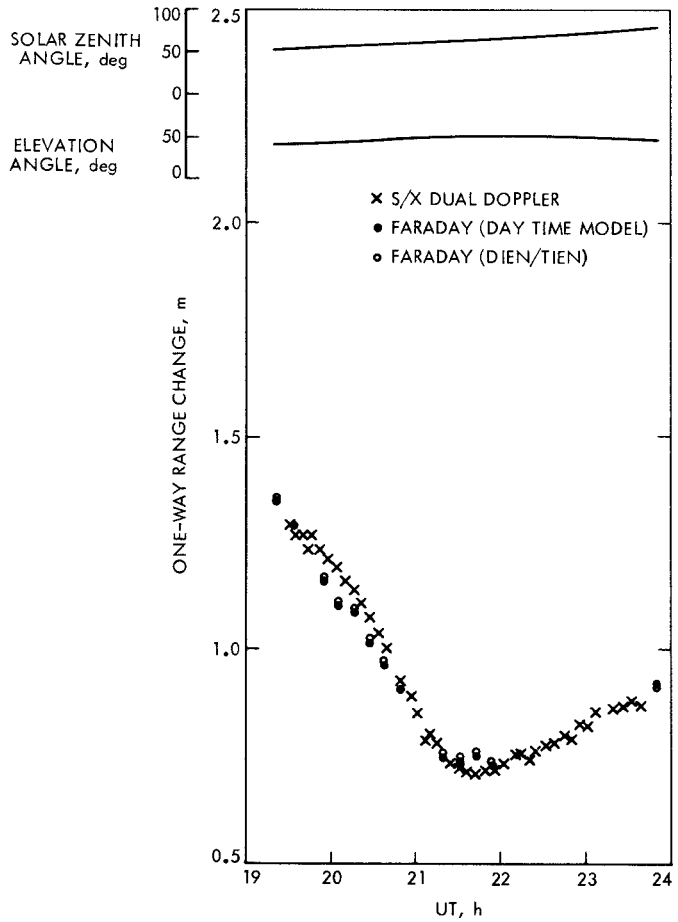

Fig. 5. Comparison of daytime ionospheric one-way range changes on Jan. 3, 1974

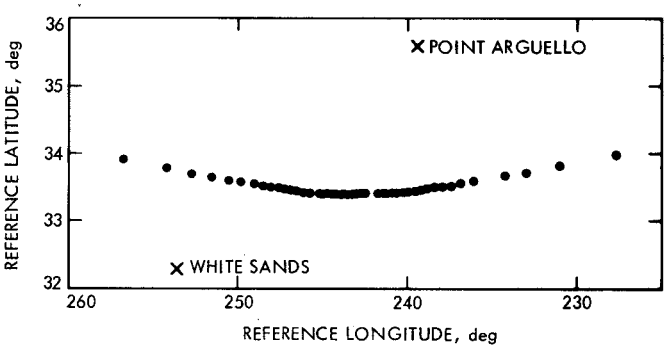

Fig. 6. Variation of ionospheric reference coordinates on Dec. 15, 1973

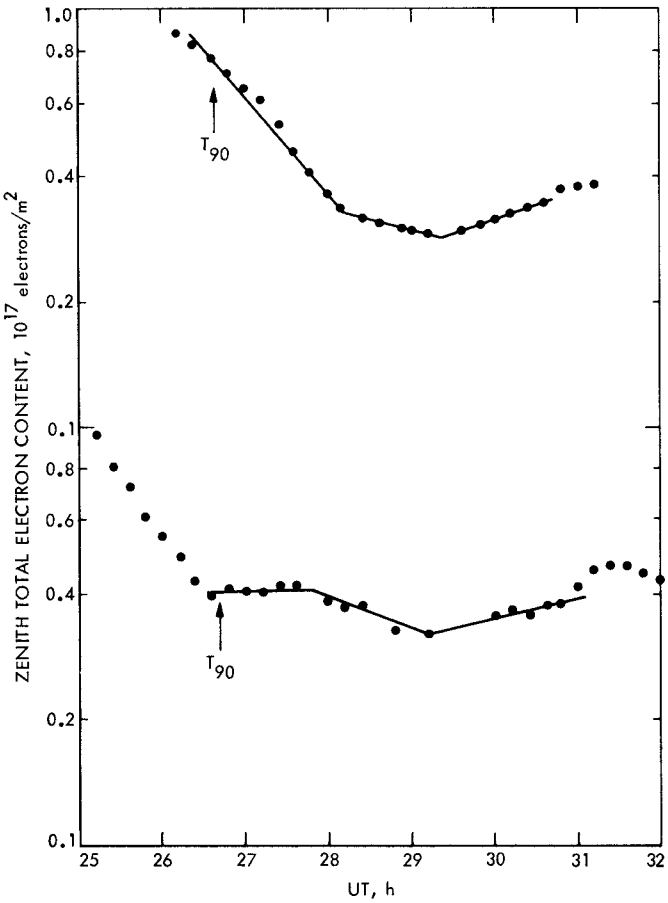

Fig. 7. Nighttime zenith total electron content at Goldstone, Calif., on Nov. 11 and 12, 1971

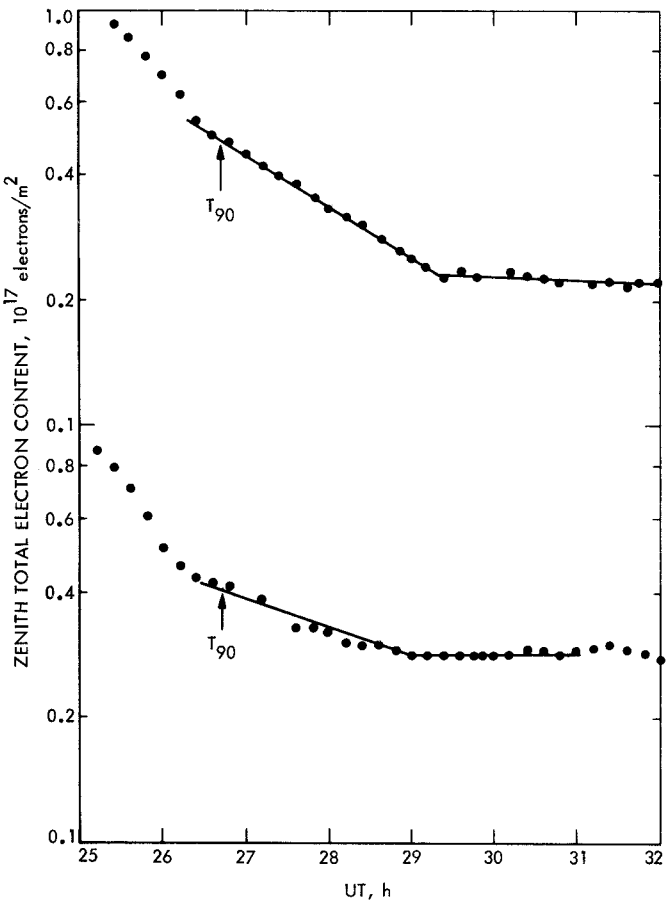

Fig. 8. Nighttime zenith total electron content at Goldstone, Calif., on Nov. 13 and 14, 1971

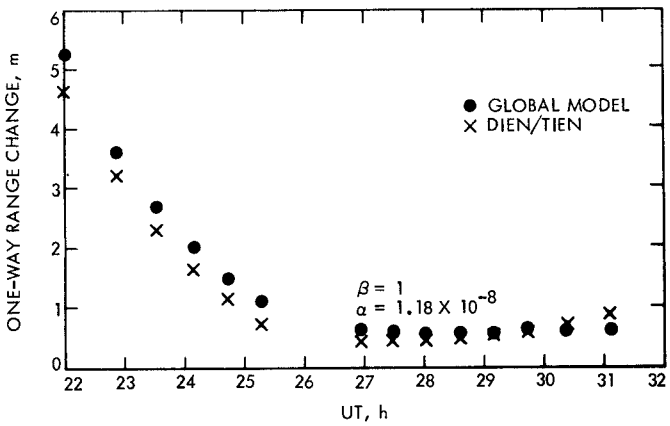

Fig. 9. Comparison of ionospheric one-way range changes on Nov. 11, 1971

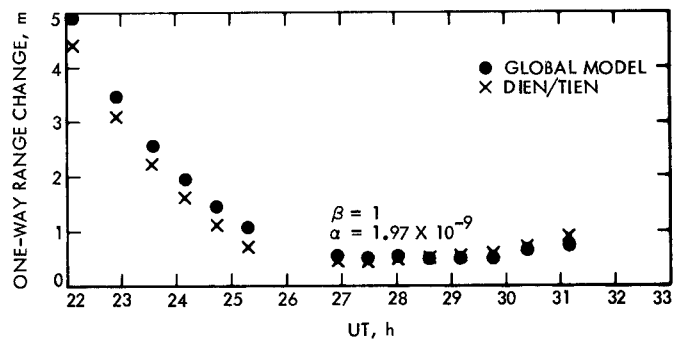

Fig. 10. Comparison of ionospheric one-way range changes on Nov. 13, 1971

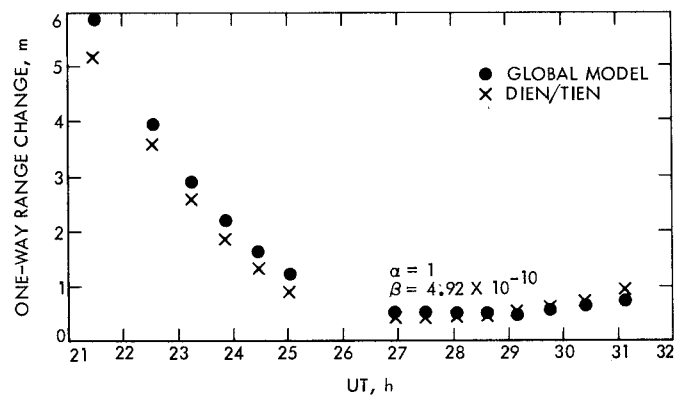

Fig. 11. Comparison of ionospheric one-way range changes on Nov. 14, 1971